Polarization-Insensitive, Broadband, and Tunable Terahertz Absorber Using Slotted-Square Graphene Meta-Rings

Subhan Zakir, Rana Muhammad Hasan Bilal, Muhammad Ashar Naveed, Muhammad Abuzar Baqir, Muhammad Usman Ali Khan, Muhammad Mahmood Ali, Muhammad Ahsan Saeed, Muhammad Qasim Mehmood, and Yehia Massoud

***Abstract*—Graphene-based metamaterials are gaining popularity for developing various reconfigurable and electrically tunable optical devices – especially in terahertz (THz) and infrared (IR) bands. Therefore, in this paper, we aim to investigate the broadband metamaterial-based absorber that efficiently absorbs the THz radiation ranging from 2.2 to 4.6 THz. The proposed absorber comprises a simple meta-square ring of graphene, which possesses different slots in its structure to induce multiple plasmonic resonances. It is observed that the proposed absorber manifests above 95% absorption for the normally incident THz waves, and it also maintains its absorption value over 80% for different obliquely incident operating conditions. Furthermore, the proposed absorber shows polarization-insensitive features. In addition, the absorption characteristics regulate from 95% to 15% by adjusting the chemical potential of graphene from 1 eV to 0.1 eV. Some of the salient features of the proposed absorber is largest reported bandwidth for single layer absorber with smallest footprint without sacrificing polarization insensitivity or amplitude tunability. From the application point of view, it could provide the pathway for implementing switching, cloaking, smart absorbers, and detection phenomena in the THz range.**

***Index Terms*—Terhertz, broadband, polarization-insensitive metamaterial, absorber, graphene, tunable.**

Manuscript received 12 October 2022; revised 29 November 2022; accepted 12 December 2022. Date of publication 20 December 2022; date of current version 28 December 2022. *(Corresponding authors: Muhammad Qasim Mehmood; Yehia Massoud.)*

Subhan Zakir is with the School of Electrical, Computer and Energy Engineering, Arizona State University, Tempe, AZ 85287 USA (e-mail: szakir1@asu.edu).

Rana Muhammad Hasan Bilal, Muhammad Ashar Naveed, and Yehia Massoud are with the Innovative Technologies Laboratories (ITL), King Abdullah University of Science and Technology (KAUST), Thuwal 23955, Saudi Arabia (e-mail: hasanbilal00@gmail.com; ashargill106@gmail.com; yehia.massoud@kaust.edu.sa).

Muhammad Abuzar Baqir is with the Department of Electrical and Computer Engineering, COMSATS University Islamabad, Punjab 57000, Pakistan (e-mail: abuzar@cuisahiwal.edu.pk).

Muhammad Usman Ali Khan is with the Department of Electronic Engineering, The Islamia University of Bahawalpur, Punjab 63100, Pakistan (e-mail: usman.ali@iub.edu.pk).

Muhammad Mahmood Ali is with the Department of Mechatronic Engineering, Atlantic Technological University, F91 YW50 Sligo, Ireland (e-mail: muhammad.ali@atu.ie).

Muhammad Ahsan Saeed is with the School of Electrical Engineering, Korea University, Seoul 02841, Korea (e-mail: ahsansaeed@korea.ac.kr).

Muhammad Qasim Mehmood is with the MicroNano Lab, Electrical Engineering Department, Information Technology University of the Punjab, Lahore 54600, Pakistan (e-mail: qasim.mehmood@itu.edu.pk).

Digital Object Identifier 10.1109/JPHOT.2022.3229900

I. Introduction

METAMATERIALS are artificially engineered materials containing sub-wavelength structures, which have become immensely popular due to their attributes such as negative refractive index [1], [2], optical cloaking [3], imaging [4], [5], polarization-conversion [6], optical reflectors [7], [8], superlensing [9], EM wave absorption [10], [11], intelligent devices [12] [13], [14] and analog computing [15], etc. The EM wave absorption characteristic of these artificial periodic structures is of particular interest due to its application in solar photovoltaics, radar cross-section reduction (RCSR), EM interference mitigation, multiple-input multiple-output (MIMO) antenna isolation, stealth technology, and other wireless communication systems [16], [17], [18]. Since the invention of the perfect metamaterial absorber in 2008 [19], metamaterial absorbers (MMAs) have attracted great status in the electromagnetic communities. These MMAs have surpassed the conventional Salisbury screen absorbers due to their superior features such as ultrathin geometry, lightweight, large bandwidth, and easily-fabricable design architecture. Henceforth, these features make MMAs a perfect candidate to tackle the current challenges of low profile, large bandwidth, and high efficiency in both microwave and optical regimes [9], [20], [21], [22], [23], [24], [25].

Recently, with the increase in the demand for high data rates and spectrum crowding, the THz band has become the center of attention of the research and development community [26]. The THz band (0.1 THz to 10 THz) has been gaining an immense reputation due to its applications in communication, sensing, imaging, and security [27], [28]. However, researchers have been facing design challenges in the THz band due to the unavailability of naturally existing materials in this region. Metamaterials offer appealing solutions to resolve the problems of narrow bandwidth, bulky size, and complex fabrication for developing modern optical and photonic devices. The EM waves can be manipulated by designing an appropriate metamaterial structure and varying the design parameters. To date, various devices in the microwave and optical regimes have been developed by exploiting the features of the metamaterials [29], [30], [31], [32], [33], [34], [35], [36].

The basic working principle of the MMAs is to confine and restrict EM waves inside the lossy materials. The transmission is usually blocked with a metal layer at the bottom of the MMAs. The large operational bandwidth of the MMAs is of significant interest in practical applications such as solar energy harvesting and bolometers [32], [33]. In literature, different techniques have been proposed to achieve the broadband response of the MMAs. One of the techniques is to use the multi-resonance approach. Meta-molecules of different geometries or sizes having resonances at different frequencies combine in a single unit cell to produce continuous wideband spectra [37]; this makes the unit cell too large; therefore, it faces difficulty in fabrication. Another technique is to use multi-layer structures separated by dielectric layers [38], which makes the absorber bulky and expensive. The other prominent technique is to use fractal structures; these are self-similar and repeated resonators arranged in a particular pattern. They generate multiple resonance phenomena owing to their repeated elements [39], [40]. However, these approaches suffer from large complex fabrication processes, making them undesirable for advanced communication systems. Based on operating bandwidth, MMAs can be described into two types, i.e., narrowband and wideband absorbers, etc. Narrowband MMAs are employed for sensing, and filtering applications [41], [42], whereas wideband MMAs contain several applications in RCSR, stealth, and solar thermophotovoltaics [39], [43], [44]. In this context, graphene-based MMAs are of particular interest due to graphene's intriguing electrical and mechanical properties. Graphene is a promising candidate for THz devices since the graphene plasmon frequency and the graphene nanoribbons' bandgap lies in the THz range [45], [46]. Graphene plasmonics has opened a new avenue in reconfigurable metasurfaces and metamaterials. Graphene contains a single layer of carbon atoms organized in a honeycomb-like structure. The Fermi level of graphene can be changed by applying an external gate voltage, which gives graphene an advantage over other materials. Although a lot of work has been done on graphene-based MMAs, they still suffer from drawbacks such as large footprint, complex structure, angle dependency, decreased absorptivity, and polarization sensitivity. In [57] authors propose a graphene disk and square ribbon-based absorber. The absorber operates in the 1.482-3.655 THz range with an absorption level of 90%. Even though the operating range is close to our proposed work, the footprint of the unit cell is 16 times larger and the absolute bandwidth is 0.23 THz smaller than our proposed work. The amplitude tunability is very poor since even after changing the chemical potential, the absorber remains above 80% in more than half of the operating band.

In the present communication, we aim to investigate the broadband THz metamaterial absorber composed of a simple slotted-square ring of graphene. The proposed graphene slotted-square metamaterial absorber (GSSMA) contains a single-layer device configuration (metal-dielectric-metal), which holds a top graphene layer mounted over a gold-backed polyimide lossy dielectric substrate. The presented absorber expresses outstanding absorption characteristics over a large operating band starting from 2.2 to 4.6 THz, and its performance also remains stable under the influence of the different obliquity of incident angles for both the transverse electric (TE) and transverse magnetic (TM) waves' excitation. To validate the polarization-insensitivity of this THz absorber, absorption spectra are also studied for various polarization angles of the EM waves, and it performs equally for all the polarization angles. Moreover, the absorptivity tunes from 100% to 15% by altering the top graphene layer's chemical potential from 1 eV to 0.1 eV. This work's major contribution and novelty are as follows: 1) largest bandwidth reported for any single layer metamaterial absorber report in the literature according to the author's knowledge. 2) Smallest footprint of the meta-atom compared to the other single-layer metamaterial absorbers in the literature. 3) Simple geometry and easy fabrication process compared to multi-layer absorbers 4) the above-mentioned features are archived without compromising the outstanding attributes such as amplitude-tunability, polarization insensitivity, and wide angular stability.

II. Absorber Theory and Design Methodology

The phenomena of absorption of EM waves can be explained by transmission line theory. MMAs are designed in such a way that its impedance matches the impedance of the incoming EM waves. As a result, there is no reflection of EM wave incidence on the MMA surface. Further, the imaginary part of the substrate's refractive index should be as large as possible to absorb the EM waves in the MMA. The absorption through MMAs can be calculated as follows [39].

$$A(\omega) = 1 - R(\omega) - T(\omega) \quad (1)$$

In (1), $A(\omega)$ represents the absorption, $R(\omega)$ represents the reflection, and $T(\omega)$ is the transmission coefficient of the MMA. The reflection and transmission coefficients in (1) can also be expressed using scattering parameters as:

$$A(\omega) = 1 - |S_{11}(\omega)|^2 - |S_{21}(\omega)|^2 \quad (2)$$

Since the bottom layer of the proposed MMA is gold, therefore, the transmission through MMA is zero, i.e., $|S_{21}(\omega)|^2 \approx 0$. (2) can be modified as:

$$A(\omega) = 1 - |S_{11}(\omega)|^2 \quad (3)$$

Fig. 1 shows the schematic of the unit cell of the proposed GSSMA. The top layer consists of a mono-layer graphene-based slotted-square-shaped meta-unit cell. The bottom layer is a continuous metallic ground made up of (t_g) = 0.2 µm thick gold, ensuring no EM waves transmission. The conductivity of gold, calculated through the Drude model with plasma frequency ω_p is $4.35\pi \times 10^{15}$ rad/s and collision frequency ω_c is $13\pi \times 10^{12}$ rad/s. The top and bottom layers sandwich a (t_d) = 12 µm thick polyimide dielectric with a relative permittivity of 3.5. The remaining optimum design parameters of the proposed absorber are as follows: periodicity of the unit cell (P) = 10 µm, length of the graphene slotted square patch (L) = 8 µm, length of the diagonal slot (L_d) = 2.63 µm, width of the diagonal slot (W_d) = 0.75 µm, length of the centered slot (L_c) = 0.75 µm and width of the centered slot (W_c) = 0.1 µm. The graphene meta-unit cell's chemical potential and relaxation time are initially selected to be 1 eV and 0.1 ps, respectively. The surface conductivity σ_{gra} of the graphene is modeled using the Kubo formula, which includes both the intraband σ_{intra} and interband σ_{inter} transitions [47],

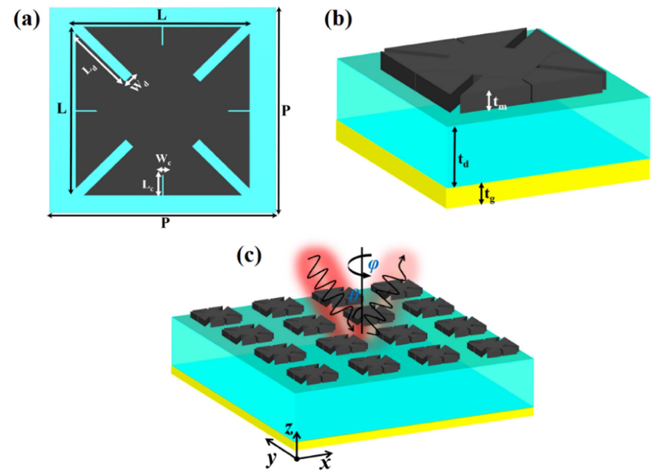

Fig. 1. Schematic illustration and design setup of the proposed GSSMA along with the representation of its geometric parameters (a) the unit cell schematic of the proposed GSSAM, (b) side view representation of the proposed GSSMA and (c) depiction of the periodic arrays of the proposed GSSMA, θ and ϕ highlight the incident and polarization angle of the EM THz waves.

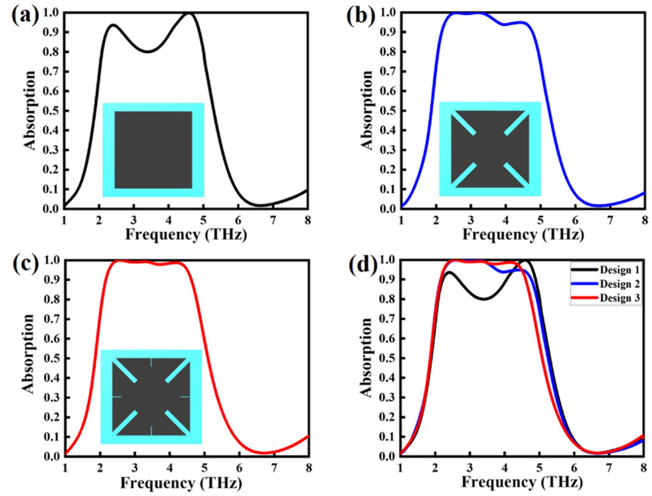

Fig. 2. Design stages of the proposed GSSMA along with its absorption performance (a) simple square patch and its corresponding absorption features (b) diagonal-slotted patch and its corresponding absorption features (c) diagonal and centered slotted patch and its corresponding absorption features and (d) comparative analysis of the absorption performance of all the design stages.

[48].

$$\begin{aligned}\sigma_{gra} &= \sigma_{intra} + \sigma_{inter}\\ &= \frac{2e^2 k_B T}{\pi\hbar^2}\frac{i}{\omega + i/\tau}\ln\left[\left(2\cosh\frac{E_f}{2k_B T}\right)\right]\\ &\quad + \frac{e^2}{4\hbar^2}\left[\frac{1}{2} + \frac{1}{\pi}\arctan\left(\frac{\hbar\omega - 2E_f}{2k_B T}\right)\right.\\ &\quad \left. - \frac{i}{2\pi} ln\frac{(\hbar\omega + 2E_f)^2}{(\hbar\omega - 2E_f)^2 + 4(k_B T)^2}\right] \end{aligned} \tag{4}$$

In (4), ω denotes the angular frequency, E_f denotes the Fermi level, τ and T are the relaxation time and absolute temperature, respectively. The constants k_B, e and $\hbar$ are Boltzmann constant, charge of an electron, and reduced Plank constant, respectively.

Unlike the visible regime, in the THz range, the Fermi energy is greater than the photon energy ($\hbar\omega\,''2E_f$). Equation (4) can be reduced to a Drude model for graphene by assuming $E_f'' k_B T$ [49], [50]

$$\sigma_{gra} = \frac{2e^2 E_f}{\pi\hbar^2}\frac{i}{(\omega + \frac{i}{\tau})} \tag{5}$$

For the design of the GSSMA, the frequency domain solver is used in the simulation to calculate the EM response and field distribution. The boundary conditions were set to have unit cells on both the x-direction and y-direction with Floquet ports on the positive and negative z-direction. The simulations were performed in CST Microwave studio. In order to simulate graphene as a single layer of carbon atoms, it is modeled with a negligible thickness (0.9 nm).

III. Results and Discussion

In this section, we characterize the performance of the proposed GSSMA by exciting it with a plane wave in the terahertz regime. The metasurface is first subjected to normal transverse

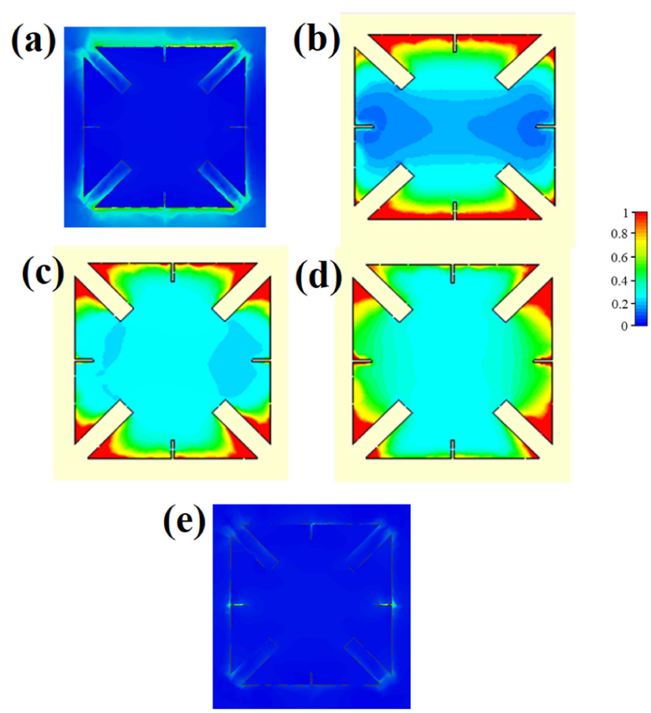

Fig. 3. Surface electric field on the top surface of the proposed GSSMA for TE mode at normal incidence at (a) 1.5 THz, (b) 2.2 THz, and (c) 3.5 THz, (d) 4.6 THz and (e) 6 THz.

electric (TE) and transverse magnetic (TM) incidences. The chemical potential of the graphene is set as 1 eV, and the relaxation time is assumed to be 0.1 ps. The unit cell design starts with a simple square graphene patch, as depicted in the inset of Fig. 2(a). The absorption level of the square patch is observed, as shown in Fig. 2(a). In a square patch MMA, the wave diffraction from the diagonals excites the transverse magnetic harmonics of 210 modes. We enhanced the absorption level by exploiting the

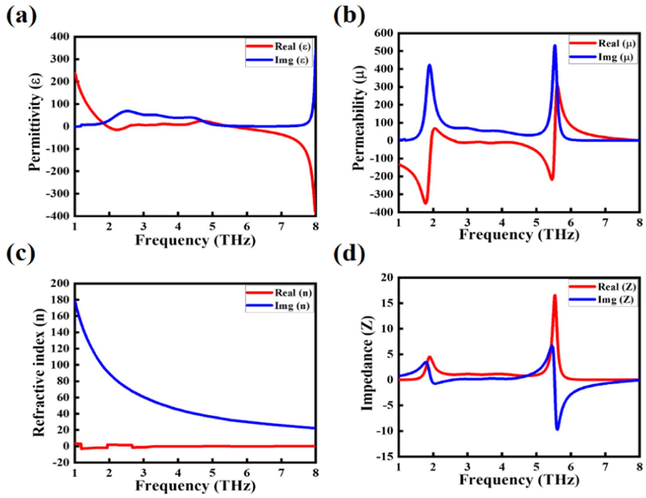

Fig. 4. Effective parameters of proposed GSSMA (a) effective permittivity, (b) effective permeability (c) effective refractive index, and (d) effective impedance.

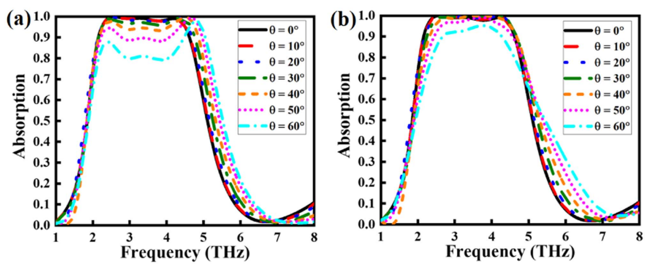

Fig. 5. Absorption features of the proposed GSSMA under different oblique incident angles of the EM THz wave (a) TE wave illumination and (b) TM wave illumination.

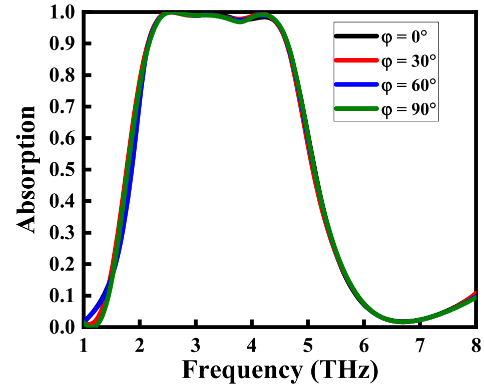

Fig. 6. Absorption features of the proposed GSSMA under different polarization angles of the EM THz wave at normal incident.

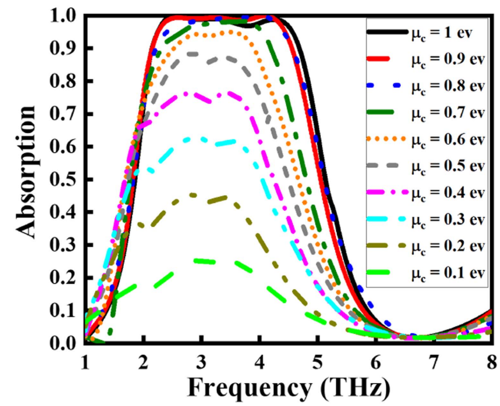

Fig. 7. Absorption features of the proposed GSSMA under different chemical potentials ($\boldsymbol{\mu_c}$) of the top graphene metasurface at the normal incident.

diagonal edges of the square patch, as presented in Fig. 2(b). Adding the slots at the diagonals achieves stronger absorption throughout the band. The diagonal slots also maintained the four-fold symmetry of the design for similar performance under TE- and TM-polarization. The overall absorption is further improved by adding slots at the center of each side of the patch, as illustrated in Fig. 2(c). Fig. 2 captures the design process and performance of the engineered GSSMA over a frequency range of 1 to 8 THz.

Fig. 3(a)–(e) show the surface electric field of the GSSMA for the different operating frequencies, namely, 1.5, 2.2, 3.5, 4.6, and 6 THz, respectively. From Fig. 3(a) and (e), we can see that there is no resonance at 1.5 THz and 6 THz since both are outside the band. Therefore, no electric field intensity is gathered at the surface of the graphene-based ring. In contrast, it is clearly noticed that electric field is maximally confined on the edges of the unit cell of the absorber for remaining operating frequencies. Further, the dipole formation is observed in Fig. 3(b) for the operating frequency 2.2 THz. Whereas the quadruple field can be seen for 3.5 and 4.6 THz as in Fig. 3(c) and (d), respectively. These dipole and quadruple lead to the electric resonance that causes the absorption.

The designed GSSMA manifests a broadband absorption response over a wide frequency spectrum starting from 2.2 to 4.6 THz with an absorption level of above 97% and a fractional bandwidth of 70%. The nearly perfect absorption results from the wideband impedance matching between free space and the metasurface at desired frequency band, which results in almost zero reflection coefficient and the gold layer at the bottom with thickness greater than the skin depth of the incident THz wave to suppress the transmission to zero. The reflection coefficient under normal incidence can be calculated using the following equation [51]:

$$\Gamma(\omega) = \frac{Z_M - Z_o}{Z_M + Z_o} \tag{6}$$

The impedance of the GSSMA is represented as Z_M and it depends on the frequency, whereas the impedance of the free space is given as Z_o. The following equations give these impedances:

$$Z_M = \sqrt{\frac{\mu_M \mu_o}{\varepsilon_M \varepsilon_o}} \tag{7}$$

$$Z_o = \sqrt{\frac{\mu_o}{\varepsilon_o}} = 377\,\Omega \tag{8}$$

TABLE I
COMPARISON OF THE PREVIOUSLY REPORTED GRAPHENE BASED ABSORBERS WITH THE PRESENT STUDY

Design configuration	Bandwidth (THz) A ≥ 90%	Tunability parameter	Unit cell size (μm^3)	Fractional bandwidth	Angular stability
Single-layer [57]	2.17	Frequency	40×40×21.5	85%	TE(θ = 30°) TM(θ = 30°)
Single-layer [58]	2.1	Frequency	80×80×20	102.8%	TE(θ = 75°) TM(θ = 75°)
Single-layer [59]	0.46	Frequency	15×15×28	32.6%	TE(θ = 60°) TM(θ = 60°)
Multi-layer [60]	2.68	Amplitude	118×118×69.2	121.8%	TE(θ = 45°) TM(θ = 65°)
Multi-layer [61]	2.57	Not given	73×73×50	140%	TE(θ = 40°) TM(θ = 50°)
Single-layer [62]	1.66	Amplitude	35×35×18	65.6%	TE(θ = 50°) TM(θ = 50°)
Multi-layer [63]	1.96	Amplitude	71×71×23.5	63.6%	TE(θ = 50°) TM(θ = 50°)
Single-layer [64]	2.17	Amplitude	69.5×69.5×22.5	97.5%	TE(θ = 50°) TM(θ = 30°)
Multi-layer [65]	1.26	Amplitude	100×100×57.5	106.7%	TE(θ = 50°) TM(θ = 45°)
Single-layer (This work)	2.4	Amplitude	10×10×12.2	70.5%	TE(θ = 60°) TM(θ = 60°)

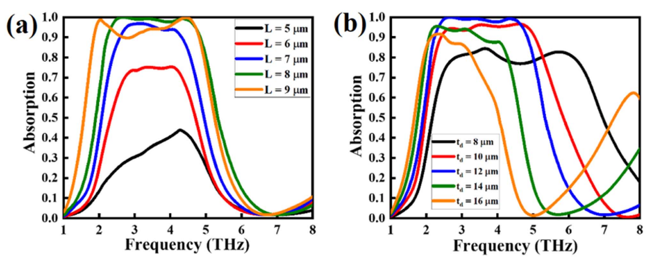

Fig. 8. Absorption features of the proposed GSSMA under different design parameters (a) Length of the GSSMA (L) and (b) Spacer thickness of the GSSMA (t_d).

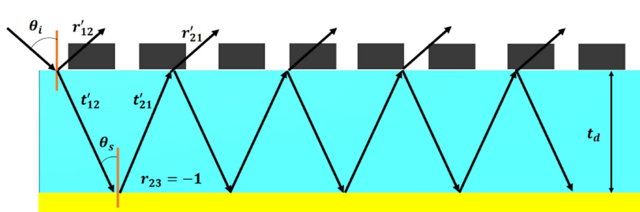

Fig. 9. Multi-reflection theory (interference) model of the proposed GSSMA. $\boldsymbol{r'_{12}}$ is the complex reflection coefficient at air-substrate interface. $\boldsymbol{t'_{12}}$ is the complex transmission coefficient of light entering the substrate from the air. $\boldsymbol{r_{23}}$ is the reflection coefficient at the substrate-bottom metal interface and $\boldsymbol{t_d}$ is the thickness of the substrate.

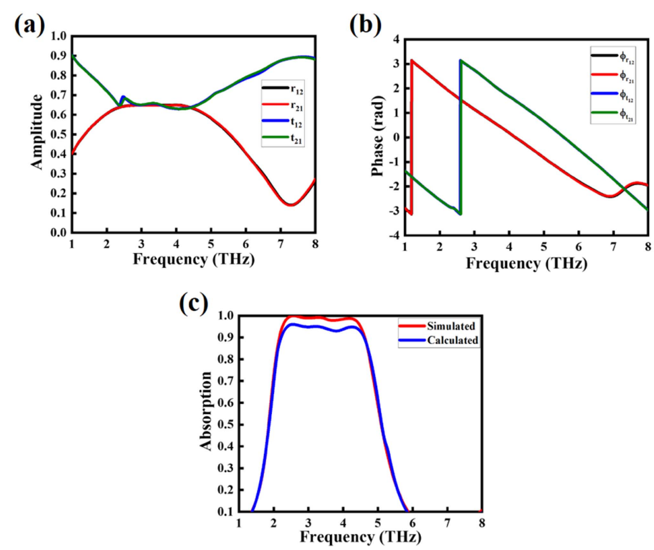

Fig. 10. Calculated results from multiple reflection theory (interference model) of the proposed GSSMA (a) amplitude spectra of the proposed GSSMA, (b) phase spectra of the proposed GSSMA, and (c) comparison between simulated and calculated absorption spectra of the proposed GSSMA.

In the above equation, ε_o and μ_o represent the permittivity and permeability of free space while ε_M and μ_M represent the effective permittivity and permeability of the GSSMA, respectively. The permittivity and permeability of the GSSMA are related to the reflection and transmission coefficients as follows [52].

$$\varepsilon_M = \frac{2}{\sqrt{-kd}} \frac{1-(S_{21}+S_{11})}{1+(S_{21}+S_{11})} \tag{9}$$

$$\mu_M = \frac{2}{\sqrt{-kd}} \frac{1-(S_{21}-S_{11})}{1+(S_{21}-S_{11})} \tag{10}$$

Where d is the height of the substrate and k is the wavenumber and $k = \omega/c$. As S_{11} and S_{21} goes to zero, ε_M and μ_M becomes equal and Z_M from (7) is matched to Z_o. The identical response for both TE and TM modes is attributed to the symmetry of the design.

In order to fully characterize the designed GSSMA, material parameters such as relative permittivity, relative permeability, loss tangent, and refractive index are extracted using s-parameters. Once the s-parameters are obtained through simulating the surface, these parameters can be calculated using the expression as [53], [54].

$$n = \frac{-iln\left(e^{ink_0 d}\right)}{k_0 d} \tag{11}$$

$$e^{ink_0d} = X \pm i\sqrt{1 - X^2} \quad (12)$$

$$X = \frac{1}{2S_{21}\left(1 - S_{11}^2 + S_{21}^2\right)} \quad (13)$$

In the above set of equations (11)–(13), k_0 and d represent the wavenumber and thickness of the absorber, respectively, and n is the refractive index of the GSSMA. The relative permittivity ε_r, relative permeability, μ_r, can be computed as follows [55], [56].

$$\varepsilon_r = \frac{n}{Z} \quad (14)$$

$$\mu_r = nZ \quad (15)$$

The Fig 4(a) and (b) show the real and imaginary values of the relative permittivity (ε_r), relative permeability (μ_r) respectively, and Fig. 4(c) illustrates the complex values of the refractive index. The impedance of the GSSMA depends on the relative permittivity (ε_r) and relative permeability (μ_r). As discussed before, the impedance of the GSSMA is given by $Z_M = \sqrt{\frac{\mu_M \mu_o}{\varepsilon_M \varepsilon_o}}$ (where ε_M and μ_M represent the permittivity and permeability of the GSSMA, respectively).

If relative permittivity and permeability of the metasurface are equal, the normalized impedance Z/Z_o of the GSSMA is unity which fulfills the matching condition for perfect absorption. For the discussed MMA, the relative permittivity and relative permeability are identical to each other in the band of interest as shown in Fig. 3(a) and (b). Since the ε_r and μ_r depend on the s-parameters, the normalized effective impedance of the surface is given by the equation [51]. Fig. 4(d) demonstrates that close to the unity normalized effective impedance of the proposed MMA.

$$Z_{eff} = \sqrt{\frac{\left(1 + S_{11}\right)^2 - S_{21}^2}{\left(1 - S_{11}\right)^2 - S_{21}^2}} = \frac{1 + S_{11}}{1 - S_{11}} \quad (16)$$

The real and imaginary part of the permittivity leads to the calculation of another important characterization parameter, i.e., loss tangent. The loss tangent of the GSSMA can be computed using the following expression [39].

$$tan\delta = \frac{Im\left(\varepsilon_r\right)}{Re\left(\varepsilon_r\right)} \quad (17)$$

Generally, the absorptivity of MMAs reduces with the obliquity of incident EM waves. The expression of the reflection coefficient for TE- and TM-polarization is given, respectively [54], [55].

$$\Gamma_{TE}\left(\omega\right) = \frac{Z_M \cos\theta_i - Z_o \cos\theta_t}{Z_M \cos\theta_i + Z_o \cos\theta_t} \quad (18)$$

$$\Gamma_{TM}\left(\omega\right) = \frac{Z_M \cos\theta_t - Z_o \cos\theta_i}{Z_M \cos\theta_t + Z_o \cos\theta_i} \quad (19)$$

In the above (18) and (19), θ_i and θ_t are the incident and the transmitted angles, respectively.

The zero-reflection condition breaks for the obliquity of incidence that causes an increase of anisotropy of the structure. The increase in the anisotropy with the increasing θ_i, changes the impedance of the surface and the equality of ε_M and μ_M breaks. The meta-atoms impedance is no longer matched with the incoming EM waves. Consequently, the absorption decreases with the increasing mismatching. However, the proposed metasurface is engineered to demonstrate wide-angle stability for robust applications. The angle stability is an account of the design simplicity (shown in Fig. 5), which results in a steady rise in anisotropy with θ_i. The designed GSSMA displays an absorption level of above 90% for an incident angle of 40° and 50° for TE- and TM-polarization, respectively. Fig. 5 shows that the absorption is above 75% for an incident angle of 60° throughout the band for both TE and TM modes.

Next, the absorptivity of GSSMA is analyzed for different polarization of incidence EM waves. The proposed GSSMA exhibits polarization insensitivity. The polarization of the normal incident EM waves is varied from 0° to 90° with a step size of 30°, and the absorption phenomenon is studied as shown in Fig. 6. It is evident from Fig. 6 that our discussed GSSMA shows no variations corresponding to the polarization angles. The reason for polarization-insensitivity is the four-fold symmetry of our design [21], [51]. As the polarization angle of the incoming wave changes, the orientation of the induced plasmonic modes also changes, but owing to the design's vertical and horizontal symmetry; the absorption level remains unaffected.

The amplitude of absorption of the GSSMA can be tuned throughout the band by changing the chemical potential (μ_c) of the graphene, as shown in Fig. 7. As the chemical potential is reduced from 1 to 0.1 eV, the absorption level reduces from above 95% to less than 20%; however, the maximum absorption is attained for $\mu_c = 0.9$ eV. This behavior of the GSSMA is similar to a switch that can be controlled using the chemical potential. High-speed digital circuits require the implementation of fast logic gates. Since the proposed device could be useful for a controllable switch, one application of such a surface is the implementation of high-frequency switching circuits and Boolean logic. The amplitude tunability of the proposed GSSMA over the wideband spectrum is obvious in Fig. 7.

The various design parameters of the proposed GSSMA are considered to attain the optimum performance. For this purpose, two major geometric parameters, length of the top graphene ring (L) and spacer thickness (td), are investigated. We first analyze the impact of the length of the GSSMA. Since the length of the unit cell is around 0.11λ, the unit cell is more like a lumped component instead of a transmission line. As we decrease the length from 8 µm, the absorption starts to decrease since the impedance of the unit cell changes. A similar effect is observed when we increase the length. Next, we analyze the effect of dielectric thickness on the absorption spectrum. The thickness of the dielectric is inversely proportional to the capacitance of the unit cell. As we increase the dielectric thickness, the capacitance decreases, and vice versa. This disturbs the impedance of the meta-atom, and we lose the resonance condition.

IV. Interference Theory

A multi-reflection-based interference theory is implemented for a more detailed analysis of the proposed GSSMA's absorption characteristics. In this theory, GSSMA was supposed to be a Fabry-Pérot like an interferometer that produces multiple resonances inside the cavity model, as illustrated in Fig. 9.

In the following model, the top arrays of graphene slotted square serve as impedance tuning resonators, and the gold metal plate beneath the dielectric substrate behaves as a perfect mirror for incoming THz waves. Let's assume this system as a decoupled model because of the existence of minor near-field interaction between the top graphene surfaces and lower metallic sheets. The top graphene surfaces and bottom gold plate were considered to be very thin surfaces (zero thickness).

When an incoming light wave interacts with the air-spacer interface, it breaks down into partially transmitted and reflected waves, as displayed in Fig. 8. Their corresponding coefficients can be written mathematically as: $r'_{12} = r_{12}e^{i\varphi_{\mathrm{r}12}}$ and $t'_{12} = t_{12}e^{i\varphi_{\mathrm{r}12}}$. The transmitted component strikes the ground metallic film and reflects back to the dielectric medium with -1 reflection parameter due to no transmission through the gold metal and has a complex propagation phase $\beta = nk_o t_d$, where t_d and k_o are thickness of the substrate and free-space wavenumber, respectively. A similar partial transmission and reflection phenomenon take place with the corresponding transmitted and reflected energies of $t'_{21} = t_{21}e^{i\varphi_{\mathrm{r}21}}$ and $r'_{21} = r_{21}e^{i\varphi_{\mathrm{r}21}}$, respectively. These multistep reflections and transmissions produces a phase shift β, and destructive interference phenomena take place. Rresultantly, maximum absorption happens due to the light waves trapping inside the middle dielectric layer. The total reflected energy can be calculated by following (20) [39].

$$\boldsymbol{r} = \boldsymbol{r}'_{12} - \frac{\boldsymbol{t}'_{12}\boldsymbol{t}'_{21}\boldsymbol{e}^{\boldsymbol{i2\beta}}}{\boldsymbol{1} + \boldsymbol{r}'_{21}\boldsymbol{e}^{\boldsymbol{i2\beta}}}. \tag{20}$$

Thus, the overall absorption of the proposed GSSMA can be approximated by $\boldsymbol{A} = 1 - |\boldsymbol{r}|^2$. Fig. 10(a) and b depicts the magnitudes and phases of the transmitted and reflected light at the air-spacer interface. Fig. 10(c) compares the simulated and calculated absorption curves of the proposed GSSMA, and it is noted that both plots are in good agreement with each other.

To demonstrate the advantage of the proposed GSSMA, a comparison is made in Table I with some of the state-of-the-art broadband MMAs in the literature. Table I shows the design topology, absorption bandwidth, size, polarization-insensitivity and angular stability. Apart from the single-layer absorber with 2.4 THz bandwidth, our proposed GSSMA has several other significant contributions as well. The devised GSSMA has a simple geometry, miniaturized footprint and large bandwidth as compared to the other single-layer and multi-layer absorbers in the table.

V. Conclusion

In summary, a novel design of polarization-insensitive, amplitude-tunable, and single-layer GSSMA was explored for THz frequencies. The discussed GSSMA illustrated above 95% absorption rate for a large THz band spanning from 2.2 THz to 4.6 THz. Furthermore, it performed well under the inspection of different obliquely incident angles and demonstrated an absorption rate of more than 80% till the excitation angle of 60° for both the TE and TM wave illumination. Furthermore, the proposed THz GSSMA showed different functionalities, including large operating bandwidth, miniaturization, tuneability, and polarization-insensitivity as compared to the previously existing graphene-based THz absorbers. Furthermore, the magnitude of the absorption spectra of the proposed absorber can be tuned from minima to maxima by regulating the Fermi level of the top graphene structure. Finally, the designed absorber could offer the platform to use in various applications, including imaging, cloaking, and high-switching operation devices.

Acknowledgment

The authors would like to acknowledge the research funding to the KAUST Innovative Technologies Laboratories (ITL) from King Abdullah University of Science and Technology (KAUST).

References

[1] J. Valentine et al., "Three-dimensional optical metamaterial with a negative refractive index," *Nature*, vol. 455, no. 7211, pp. 376–379, 2008.
[2] D. Lee et al., "Hyperbolic metamaterials: Fusing artificial structures to natural 2D materials," *ELight*, vol. 2, no. 1, pp. 1–23, 2022.
[3] D. Schurig et al., "Metamaterial electromagnetic cloak at microwave frequencies," *Science*, vol. 314, no. 5801, pp. 977–980, 2006.
[4] I. Javed et al., "Broad-band polarization-insensitive metasurface holography with a single-phase map," *ACS Appl. Mater. Interfaces*, vol. 14, no. 31, pp. 36019–36026, 2022.
[5] M. A. Naveed et al., "Novel spin-decoupling strategy in liquid crystal-integrated metasurfaces for interactive metadisplays," *Adv. Opt. Mater.*, vol. 10, 2022, Art. no. 2200196, doi: 10.1002/adom.202200196.
[6] T. Ahmad et al., "Ultrawideband cross-polarization converter using anisotropic reflective metasurface," *Electronics*, vol. 11, no. 3, 2022, Art. no. 487.
[7] A. Hosseini and Y. Massoud, "A low-loss metal-insulator-metal plasmonic Bragg reflector," *Opt. Exp.*, vol. 14, no. 23, pp. 11318–11323, 2006.
[8] A. Hosseini, H. Nejati, and Y. Massoud, "Modeling and design methodology for metal-insulator-metal plasmonic Bragg reflectors," *Opt. Exp.*, vol. 16, no. 3, pp. 1475–1480, 2008.
[9] M. A. Naveed et al., "Single-step fabricable flexible metadisplays for sensitive chemical/biomedical packaging security and beyond," *ACS Appl. Mater. Interfaces*, vol. 14, no. 27, pp. 31194–31202, 2022.
[10] R. Bilal, M. Naveed, M. Baqir, M. Ali, and A. Rahim, "Design of a wideband terahertz metamaterial absorber based on pythagorean-tree fractal geometry," *Opt. Mater. Exp.*, vol. 10, no. 12, pp. 3007–3020, 2020.
[11] M. A. Abbas et al., "Nanostructured chromium-based broadband absorbers and emitters to realize thermally stable solar thermophotovoltaic systems," *Nanoscale*, vol. 14, no. 17, pp. 6425–6436, 2022.
[12] M. Q. Mehmood et al., "Single-cell-driven tri-channel encryption metadisplays," *Adv. Sci.*, 2022, Art. no. 2203962.
[13] R. Zhu et al., "Remotely mind-controlled metasurface via brainwaves," *eLight*, vol. 2, no. 1, pp. 1–11, 2022.
[14] M. Wang et al., "Spin-orbit-locked hyperbolic polariton vortices carrying reconfigurable topological charges," *eLight*, vol. 2, no. 1, pp. 1–11, 2022.
[15] A. Silva, F. Monticone, G. Castaldi, V. Galdi, A. Alù, and N. Engheta, "Performing mathematical operations with metamaterials," *Science*, vol. 343, no. 6167, pp. 160–163, 2014.
[16] H.-T. Chen, A. J. Taylor, and N. Yu, "A review of metasurfaces: Physics and applications," *Rep. Prog. Phys.*, vol. 79, no. 7, 2016, Art. no. 076401.
[17] A. Li, S. Singh, and D. Sievenpiper, "Metasurfaces and their applications," *Nanophotonics*, vol. 7, no. 6, pp. 989–1011, 2018.
[18] S. Yin, E. Galiffi, and A. Alù, "Floquet metamaterials," *eLight*, vol. 2, no. 1, pp. 1–13, 2022.
[19] N. I. Landy, S. Sajuyigbe, J. J. Mock, D. R. Smith, and W. J. Padilla, "Perfect metamaterial absorber," *Phys. Rev. Lett.*, vol. 100, no. 20, 2008, Art. no. 207402.
[20] J. Zhang et al., "Ultra-broadband microwave metamaterial absorber with tetramethylurea inclusion," *Opt. Exp.*, vol. 27, no. 18, pp. 25595–25602, 2019.
[21] R. Bilal, M. Baqir, P. Choudhury, M. Naveed, M. Ali, and A. Rahim, "Ultrathin broadband metasurface-based absorber comprised of tungsten nanowires," *Results Phys.*, vol. 19, 2020, Art. no. 103471.

[22] M. C. Tran et al., "Broadband microwave coding metamaterial absorbers," *Sci. Rep.*, vol. 10, no. 1, pp. 1–11, 2020, doi: 10.1038/s41598-020-58774-1.
[23] D. Wang et al., "Switchable ultrathin quarter-wave plate in terahertz using active phase-change metasurface," *Sci. Rep.*, vol. 5, 2015, Art. no. 15020, doi: 10.1038/srep15020.
[24] T. Cao, C. W. Wei, R. E. Simpson, L. Zhang, and M. J. Cryan, "Broadband polarization-independent perfect absorber using a phase-change metamaterial at visible frequencies," *Sci. Rep.*, vol. 4, 2014, Art. no. 3955, doi: 10.1038/srep03955.
[25] S. Ijaz, A. S. Rana, Z. Ahmad, M. Zubair, Y. Massoud, and M. Q. Mehmood, "The dawn of metadevices: From contemporary designs to exotic applications," *Adv. Devices Instrum.*, vol. 2022, 2022, Art. no. 9861078, doi: 10.34133/2022/9861078.
[26] I. F. Akyildiz, J. M. Jornet, and C. Han, "Terahertz band: Next frontier for wireless communications," *Phys. Commun.*, vol. 12, pp. 16–32, 2014.
[27] D. Dragoman and M. Dragoman, "Terahertz fields and applications," *Prog. Quantum Electron.*, vol. 28, no. 1, pp. 1–66, 2004.
[28] A. Arbabi and A. Faraon, "Fundamental limits of ultrathin metasurfaces," *Sci. Rep.*, vol. 7, 2017, Art. no. 43722, doi: 10.1038/srep43722.
[29] Y. J. Kim, Y. J. Yoo, K. W. Kim, J. Y. Rhee, Y. H. Kim, and Y. Lee, "Dual broadband metamaterial absorber," *Opt. Exp.*, vol. 23, no. 4, pp. 3861–3868, 2015.
[30] M. A. Naveed, R. M. H. Bilal, A. A. Rahim, M. A. Baqir, and M. M. Ali, "Polarization-insensitive dual-wideband fractal meta-absorber for terahertz applications," *Appl. Opt.*, vol. 60, no. 29, pp. 9160–9166, 2021.
[31] R. M. H. Bilal, M. A. Baqir, M. Hameed, S. A. Naqvi, and M. M. Ali, "Triangular metallic ring-shaped broadband polarization-insensitive and wide-angle metamaterial absorber for visible regime," *J. Opt. Soc. Amer. A*, vol. 39, no. 1, pp. 136–142, 2022.
[32] H. Wang, V. P. Sivan, A. Mitchell, G. Rosengarten, P. Phelan, and L. Wang, "Highly efficient selective metamaterial absorber for high-temperature solar thermal energy harvesting," *Sol. Energy Mater. Sol. Cells*, vol. 137, pp. 235–242, 2015.
[33] T. Maier and H. Brückl, "Wavelength-tunable microbolometers with metamaterial absorbers," *Opt. Lett.*, vol. 34, no. 19, pp. 3012–3014, 2009.
[34] S. Zhang et al., "Dynamic display of full-Stokes vectorial holography based on metasurfaces," *ACS Photon.*, vol. 8, no. 6, pp. 1746–1753, 2021.
[35] R. M. H. Bilal, M. A. Saeed, M. A. Naveed, M. Zubair, M. Q. Mehmood, and Y. Massoud, "Nickel-based high-bandwidth nanostructured metamaterial absorber for visible and infrared spectrum," *Nanomaterials*, vol. 12, no. 19, 2022, Art. no. 3356.
[36] M. D. Shafqat, N. Mahmood, M. Zubair, M. Q. Mehmood, and Y. Massoud, "Highly efficient perfect vortex beams generation based on all-dielectric metasurface for ultraviolet light," *Nanomaterials*, vol. 12, no. 19, 2022, Art. no. 3285. [Online]. Available: https://www.mdpi.com/2079-4991/12/19/3285
[37] M. Kenney, J. Grant, Y. D. Shah, I. Escorcia-Carranza, M. Humphreys, and D. R. Cumming, "Octave-spanning broadband absorption of terahertz light using metasurface fractal-cross absorbers," *ACS Photon.*, vol. 4, no. 10, pp. 2604–2612, 2017.
[38] F. Ding, Y. Cui, X. Ge, Y. Jin, and S. He, "Ultra-broadband microwave metamaterial absorber," *Appl. Phys. Lett.*, vol. 100, no. 10, 2012, Art. no. 103506.
[39] M. A. Naveed, R. M. H. Bilal, M. A. Baqir, M. M. Bashir, M. M. Ali, and A. A. Rahim, "Ultrawideband fractal metamaterial absorber made of nickel operating in the UV to IR spectrum," *Opt. Exp.*, vol. 29, no. 26, pp. 42911–42923, 2021.
[40] R. Bilal et al., "Elliptical metallic rings-shaped fractal metamaterial absorber in the visible regime," *Sci. Rep.*, vol. 10, no. 1, pp. 1–12, 2020.
[41] F. Yan, Q. Li, H. Tian, Z. Wang, and L. Li, "An ultrahigh Q-factor dual-band terahertz perfect absorber with a dielectric grating slit waveguide for sensing," *J. Phys. D: Appl. Phys.*, vol. 53, no. 23, 2020, Art. no. 235103.
[42] R. Wang et al., "Triple-band tunable perfect terahertz metamaterial absorber with liquid crystal," *Opt. Exp.*, vol. 25, no. 26, pp. 32280–32289, 2017.
[43] X. Kong et al., "Transparent metamaterial absorber with broadband radar cross-section (RCS) reduction for solar arrays," *IET Microw., Antennas Propag.*, vol. 14, no. 13, pp. 1580–1586, 2020.
[44] K. Iwaszczuk, A. C. Strikwerda, K. Fan, X. Zhang, R. D. Averitt, and P. U. Jepsen, "Flexible metamaterial absorbers for stealth applications at terahertz frequencies," *Opt. Exp.*, vol. 20, no. 1, pp. 635–643, 2012.
[45] V. Barone, O. Hod, and G. E. Scuseria, "Electronic structure and stability of semiconducting graphene nanoribbons," *Nano Lett.*, vol. 6, no. 12, pp. 2748–2754, 2006.
[46] X.-F. Wang, "Plasmon spectrum of two-dimensional electron systems with rashba spin-orbit interaction," *Phys. Rev. B*, vol. 72, no. 8, 2005, Art. no. 085317.
[47] G. W. Hanson, "Dyadic Green's functions and guided surface waves for a surface conductivity model of graphene," *J. Appl. Phys.*, vol. 103, no. 6, 2008, Art. no. 064302.
[48] H. Huang, H. Xia, W. Xie, Z. Guo, H. Li, and D. Xie, "Design of broadband graphene-metamaterial absorbers for permittivity sensing at mid-infrared regions," *Sci. Rep.*, vol. 8, no. 1, Mar. 2018, Art. no. 4183, doi: 10.1038/s41598-018-22536-x.
[49] H. Feng et al., "Tunable polarization-independent and angle-insensitive broadband terahertz absorber with graphene metamaterials," *Opt. Exp.*, vol. 29, no. 5, pp. 7158–7167, 2021.
[50] P. Sun et al., "Graphene-based dual-band independently tunable infrared absorber," *Nanoscale*, vol. 10, no. 33, pp. 15564–15570, 2018.
[51] S. Mehrabi, R. M. H. Bilal, M. A. Naveed, and M. M. Ali, "Ultra-broadband nanostructured metamaterial absorber based on stacked square-layers of TiN/TiO2," *Opt. Mater. Exp.*, vol. 12, no. 6, pp. 2199–2211, 2022.
[52] C. Hu, X. Li, Q. Feng, X. N. Chen, and X. Luo, "Investigation on the role of the dielectric loss in metamaterial absorber," *Opt. Exp.*, vol. 18, no. 7, pp. 6598–6603, 2010.
[53] L. Sun, H. Cheng, Y. Zhou, and J. Wang, "Broadband metamaterial absorber based on coupling resistive frequency selective surface," *Opt. Exp.*, vol. 20, no. 4, pp. 4675–4680, 2012.
[54] D. Lim, D. Lee, and S. Lim, "Angle-and polarization-insensitive metamaterial absorber using via array," *Sci. Rep.*, vol. 6, no. 1, pp. 1–9, 2016.
[55] R. Bilal, M. Baqir, A. Iftikhar, S. Naqvi, M. Mughal, and M. Ali, "Polarization-controllable and angle-insensitive multiband Yagi-Uda-shaped metamaterial absorber in the microwave regime," *Opt. Mater. Exp.*, vol. 12, no. 2, pp. 798–810, 2022.
[56] B.-Z. Xu, C.-Q. Gu, Z. Li, and Z.-Y. Niu, "A novel structure for tunable terahertz absorber based on graphene," *Opt. Exp.*, vol. 21, no. 20, pp. 23803–23811, 2013.
[57] A. Norouzi-Razani and P. Rezaei, "Broadband polarization insensitive and tunable terahertz metamaterial perfect absorber based on the graphene disk and square ribbon," *Micro Nanostructures*, vol. 163, 2022, Art. no. 107153.
[58] P. Upender and A. Kumar, "Graphene-based ultra-wideband absorber for terahertz applications using hexagonal split ring resonators," *Physica Scripta*, vol. 97, no. 6, 2022, Art. no. 065503.
[59] N. Mou et al., "Hybridization-induced broadband terahertz wave absorption with graphene metasurfaces," *Opt. Exp.*, vol. 26, no. 9, pp. 11728–11736, Apr. 2018, doi: 10.1364/OE.26.011728.
[60] X. Huang, M. Cao, D. Wang, X. Li, J. Fan, and X. Li, "Broadband polarization-insensitive and oblique-incidence terahertz metamaterial absorber with multi-layered graphene," *Opt. Mater. Exp.*, vol. 12, no. 2, pp. 811–822, 2022.
[61] M. Rahmanzadeh, H. Rajabalipanah, and A. Abdolali, "Multilayer graphene-based metasurfaces: Robust design method for extremely broadband, wide-angle, and polarization-insensitive terahertz absorbers," *Appl. Opt.*, vol. 57, no. 4, pp. 959–968, Feb. 2018, doi: 10.1364/AO.57.000959.
[62] D. Hu et al., "Tunable broadband terahertz absorber using a single-layer square graphene patch with fourfold rotationally symmetric groove," *Opt. Mater.*, vol. 109, 2020, Art. no. 110235.
[63] J. Xu et al., "Broadband tunable perfect absorber with high absorptivity based on double layer graphene," *Opt. Mater. Exp.*, vol. 11, no. 10, pp. 3398–3410, 2021, doi: 10.1364/ome.439348.
[64] J. Han and R. Chen, "Tunable broadband terahertz absorber based on a single-layer graphene metasurface," *Opt. Exp.*, vol. 28, no. 20, pp. 30289–30298, Sep. 2020, doi: 10.1364/OE.403631.
[65] T. Xie, D. Chen, H. Yang, Y. Xu, Z. Zhang, and J. Yang, "Tunable broadband terahertz waveband absorbers based on fractal technology of graphene metamaterial," *Nanomaterials*, vol. 11, no. 2, Jan. 2021, doi: 10.3390/nano11020269.